Biointerface Research in Applied Chemistry
Platinum Open Access Journal (ISSN: 2069-5837)

Article
Volume 11, Issue 1, 2021, 8804 - 8817
https://doi.org/10.33263/BRIAC112.88048817

A Computational Approach to Understand the Interactions Stabilizing the Aβ$_{1-42}$ Oligomers

Mary Dutta [1], Ankita Deb [1], Dorothy Das[1], Venkata Satish Kumar Mattaparthi [1]*

[1] Molecular Modelling and Simulation Laboratory, Department of Molecular Biology and Biotechnology, Tezpur University, Tezpur-784 028, Assam, India
* Correspondence: mvenkatasatishkumar@gmail.com;

Scopus Author ID 54962670000

Received: 20.07.2020; Revised: 17.08.2020; Accepted: 18.08.2020; Published: 21.08.2020

Abstract: Aβ peptide aggregation is known to be an important factor in the cause of Alzheimer's disease (AD). Smaller oligomers, the intermediates during the process of aggregation, are known to be more neurotoxic than matured fibrils. To gain the insight into the toxicity of low molecular weight Aβ$_{1-42}$ oligomers, it is essential to understand the course of its formation and the interactions involved. But the structural dynamics of Aβ$_{1-42}$ oligomers at the atomistic level and the interactions holding the monomeric units in the oligomeric structures still remain elusive. In this study, using molecular dynamics simulations, we have investigated the structural dynamics of the toxic Aβ$_{1-42}$ peptide intermediates and the interactions stabilizing the oligomers. From the structural dynamics of Aβ$_{1-42}$ oligomers, we observed the significant number of secondary structural transitions from α-helix to random coils in some of the monomeric units. From the interaction study, we noticed the involvement of hydrophobic contacts and inter-molecular hydrogen bonds in stabilizing the oligomers. Additionally, we subjected the equilibrated structure of the oligomers in the PDBSum server to examine the protein-protein interactions. The interaction results obtained from the PDBSum server was found to be consistent with the results obtained from the trajectory analysis.

Keywords: Aβ$_{1-42}$ peptide; Oligomers; Alzheimer's disease; Protein Aggregation; Protein misfolding.

© 2020 by the authors. This article is an open-access article distributed under the terms and conditions of the Creative Commons Attribution (CC BY) license (https://creativecommons.org/licenses/by/4.0/).

1. Introduction

Alzheimer's disease (AD), first described by the German psychiatrist, Alois Alzheimer, is categorized under a growing list of disorders [1] caused by β-sheet-rich insoluble filamentous deposits [2]. There is compelling evidence generated over the years that confirm Aβ peptides [3-5] to be the major stimulating factor of early onset of AD. These peptides are found in a variety of lengths, of which Aβ$_{1-42}$ is the most abundant and toxic in nature [6]. Structural investigations have reported that synaptic structure and function can be impaired even by the smallest Aβ oligomers and dimers [7-9]. Although the amyloid fibrils are not as toxic as the oligomers, they act as a reservoir of Aβ monomers. Under normal physiological conditions, small soluble oligomers are the most toxic species involved in aggregation, which leads to the formation of amyloid fibrils [10-12]. It has been shown that the characteristic soluble oligomers of Aβ$_{1-40}$ and Aβ$_{1-42}$ comprise of a mixture of dimer and tetramers which adopt secondary structure rich in β sheets and also denote the presence of oligomers consisting larger spherical particles with beta-strand structure [13-16]. The occurrences of Aβ$_{1-42}$ oligomers confined within plaques specify to the dynamic equilibrium between these species. In human neurons, Aβ$_{1-42}$ oligomers are found to be present intracellularly [17]. Determination of the

oligomerization state of Aβ on the membrane by visualizing individual Aβ species on the surface of murine hippocampal neurons has been carried out previously using total internal reflection fluorescence microscopy [18]. While there has been an increasing number of studies carried out to understand the oligomeric structures of Aβ peptide [19, 20] conclusive X-ray diffraction, or 3D NMR structure of an Aβ oligomer is yet to be determined [21]. MD simulation study carried out by Yu and colleagues in a lipid membrane environment predicted the structure of Aβ oligomers to have a hydrophobic core and hydrophilic surface [22]. Very recently, it has been shown that the α-sheet secondary structure in Aβ peptide drives aggregation and is strongly correlated with toxicity [23]. Eisenberg and co-workers prepared a novel species of amyloid oligomer with a mature cross-β structure where side chains penetrate adjacent β-sheets holding the sheets together. It has been named as a toxic amyloid-β fibrillar oligomer (TABFO) [24]. Although, TABFO's share structural similarity with the amyloid fibrils, they are not short protofilaments and cannot seed new amyloid fibrils. Various reports have demonstrated similar, but not identical oligomeric structures formed by $A\beta_{1-40}$ and $A\beta_{1-42}$ peptide with two additional amino acids in the C-terminal end of $A\beta_{1-42}$ peptide leading to a more diverse set of interactions [25, 26]. Although conformational studies on $A\beta_{1-42}$ oligomers have been carried out, yet little information is known about the initial stages of oligomerization. But there are a number of recent studies that have been focussed on the characterization of $A\beta_{1-42}$ oligomers [27-36]. In this work, we have investigated the conformational dynamics of the dimer, trimer, and tetramer of $A\beta_{1-42}$ peptide using molecular dynamics simulation and analyzed the corresponding MD trajectories to examine their interaction profile. We prepared the initial $A\beta_{1-42}$ dimer, trimer, and tetramer structure in the M-Z Dock server [37] using the NMR structure of $A\beta_{1-42}$ (PDB ID:1IYT) from Protein data bank. Moreover, using the PDBsum server [38], we investigated the interface statistics and interface residues of the $A\beta_{1-42}$ oligomers.

2. Materials and Methods

2.1. Preparation of initial monomer structure to construct Aβ oligomers.

The initial monomer structure of $A\beta_{1-42}$ peptide was retrieved from RCSB Protein Data Bank (PDB) entries: 1IYT [39]. The monomeric structure was then solvated with TIP3P water model with solvent buffer being 10 Å in all directions [40]. To neutralize the negative charge of the monomer, appropriate numbers of sodium ions were added. The system was minimized in two stages to ensure the stability wherein it was first subjected to 500 steps of steepest descents minimization followed by 500 steps conjugate gradient minimization. Here the system was constrained by 50 kcal/mol/$Å^2$ harmonic potential to remove the bad contacts. The whole system (monomer with water) was subsequently minimized using 1,000 steps of steepest descents minimization without the harmonic restraints at NVT ensemble. The system was then gradually heated from 0 to 300 K without the atomic restraints over a timescale of 20 ps. The system was switched to NPT ensemble and equilibrated for 100 ps without applying any restraint.

The bonds to the hydrogen atoms were constrained using the SHAKE algorithm [41]. Subsequently, MD was performed under constant pressure-temperature conditions (NPT) with temperature regulation achieved using Berendsen weak coupling method [42] and calculated electrostatic forces using the particle- mesh Ewald procedure (PME) [43]. The rest of the MD

simulation protocol that we followed in this work is the same as we did in our earlier work-study [44].

2.2. Construction of $A\beta_{1-42}$ oligomer structures.

The equilibrated monomer was submitted in the M-Z Dock server to construct the model dimer, trimer, and tetramer structures. In the M-Z Dock server, a grid-based Fast Fourier Transform method is used to explore the 3-D space to construct the best symmetric multimers [37]. In this server, the optimal fit between the protein units in the multimer complex is determined using the scoring function that considers surface complementarity, electrostatics, and desolvation. The Surface complementarity is computed using pairwise shape complementarity (PSC). PSC is a function of a favorable term (determined by the number of atom pairs within a particular distance cutoff) and a penalty term (determined by the number of clashes). The desolvation is computed from Atomic Contact Energy (ACE) and the electrostatics from the Coulomb's equation to the partial charges of the ligand in the Electrostatic field of the receptor. In this server, the search strategy mainly involves discretization of ligand and receptor onto a grid and then application of the FFT method to determine the best fitting position of the ligand relative to the receptor. This discretization and FFT is carried out for a complete set of angular orientations of the ligand while keeping the position of receptor fixed. The top-scoring dimer, trimer, and tetramer complexes were then selected and then solvated in the TIP3P water model, respectively, and then subjected to a two-step restrained minimization, followed by heating. Then the complexes were equilibrated for 100 ps followed by MD simulation of 50 ns for each individual complex. Such time was sufficient to obtain a stable configuration. Clustering was performed on a series of MD trajectories [45]. Trajectories were created from independent runs leading to partitioning into six clusters. After the MD run, the VMD package [46] was used for visualization of the 3D structure of the molecule.

2.3. Investigation of interface statistics and interface residues.

In order to investigate the interface statistics and interface residues of $A\beta_{1-42}$ oligomers, we have submitted the conformer representing the most populated clusters from the MD trajectories in the PDBSum server and carried out their interaction studies.

3. Results and Discussion

3.1. Conformational dynamics of $A\beta_{1-42}$ oligomers.

The initial dimer, trimer, and tetramer structure of $A\beta_{1-42}$ generated from the M-Z Dock server were shown in Figure 1. Individual monomeric chains were marked with different colors and labeled as Chain A, B, C, and D, respectively.

The conformational dynamics of $A\beta_{1-42}$ dimer obtained from MD simulation at different time intervals are illustrated in Figure 2. From the conformational changes undergone by the dimer complex in 50 ns, it can be clearly observed that most of the residues in the dimer complex underwent changes from α-helix to random coils. By using the DSSP tool [47], which determines the existence of hydrogen bonds as criteria for the presence of secondary structure, we also calculated the secondary structures of $A\beta_{1-42}$ dimer during the course of the simulation.

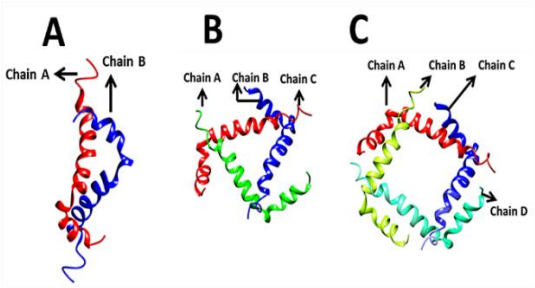

Figure 1. Initial structures generated from the M-Z Dock server: A) $A\beta_{1-42}$ dimer; B) $A\beta_{1-42}$ trimer; C) $A\beta_{1-42}$ tetramer.

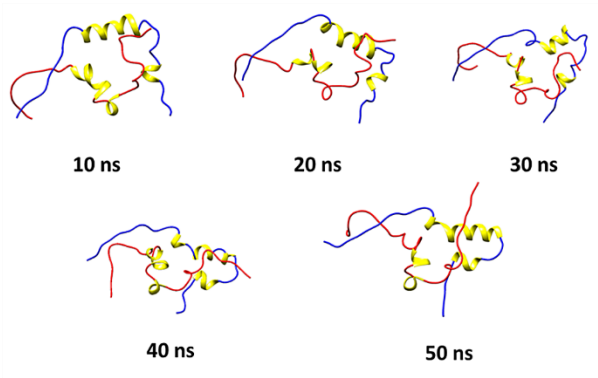

Figure 2. Conformational dynamics of $A\beta_{1-42}$ dimer at the different time course of simulation at 300 K.

The evolution of the secondary structures from the trajectories as a function of time is shown in Figure S1. We observed the appearance of β-strands at C-terminal regions in Chain B.

In the same way, snapshots of $A\beta_{1-42}$ trimer at different time intervals during the time course of simulation up to 50 ns are shown in Figure 3. From Figure 3, we can observe that individual monomeric units undergo a slow transition from the α-helical structure to random coils. Since all the three monomeric units are held together very closely, therefore secondary structural changes over the simulation time period are not drastic.

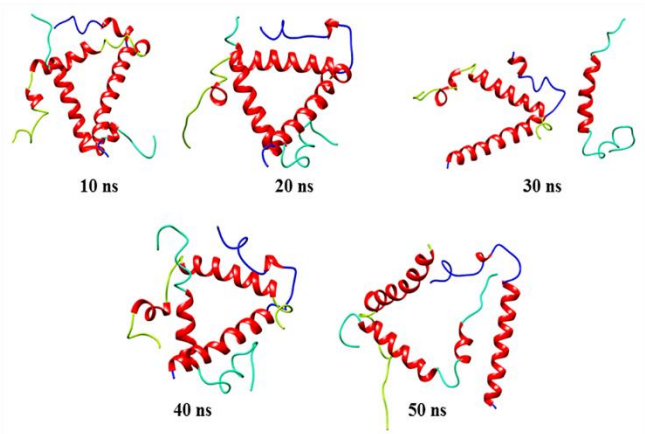

Figure 3. Conformational dynamics of $A\beta_{1-42}$ trimer at a different course of simulation at 300 K.

The evolution of the secondary structures from the trajectories as a function of time is shown in Figure S2. We observed the appearance of β-strands at C-terminal regions in Chain C, which is encircled in blue.

Similarly, the conformations of Aβ$_{1-42}$ tetramers at different time intervals are shown in Figure 4.

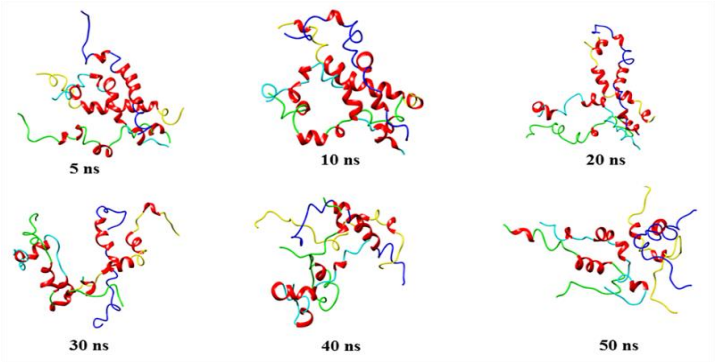

Figure 4. Conformational dynamics of Aβ$_{1-42}$ tetramer at a different course of simulation at 300 K.

In the case of Aβ$_{1-42}$ tetramer, we can observe drastic secondary structural changes from the α-helical structure to random coils and then to β-strands. Furthermore, from the evolution of secondary structural analysis using the DSSP tool of the trajectories generated from the simulation run, we observed the appearance of β-strands at C-terminal regions in the Chain D (Figure S3).

Additionally, we have compared the secondary structural contents of the initial structure and the average structure of the Aβ$_{1-42}$ dimer, trimer, and tetramer using YASARA [48], and results are summarized in Table 1. From Table 1, we can see that the initial structures of Aβ$_{1-42}$ dimer, trimer, and tetramer are rich in helical content ~70%.

Table 1. Secondary structural analysis details of Aβ$_{1-42}$ oligomers.

Secondary Structures	Aβ$_{1-42}$ Dimer		Aβ$_{1-42}$ Trimer		Aβ$_{1-42}$ Tetramer	
	Initial Structure	Equilibrated Structure	Initial Structure	Equilibrated Structure	Initial Structure	Equilibrated Structure
Helix	76.2%	14.3%	78.6%	49.2%	67.4%	19%
Sheet	0%	2%	0%	3.2%	0%	11%
Turn	0%	19%	0%	12.7%	5.4%	32%
Coil	23.8%	61.9%	21.4%	28.6%	24.5%	38%
3-$_{10}$ helix	0%	2.8%	0%	6.3%	2.7%	0%

During the time course of a simulation, all the three oligomer complexes underwent secondary structural changes, and the average structures were found to be rich in coils and turns. The helical contents that were predominant in the initial structures declined, and the beta-sheet content that was 0 % in the initial structure of Aβ$_{1-42}$ was found to increase. Thus, we can say that the oligomers that are in random coil and turn state have the tendency to acquire β-strands later.

3.2. Hydrogen bonding and hydrophobic contact analysis of Aβ$_{1-42}$ oligomers.

We have calculated the total number of intermolecular hydrogen bonds and hydrophobic contacts of the Aβ$_{1-42}$ dimer, trimer, and tetramer that play a vital role in stabilizing the oligomer structures. To calculate the hydrogen bonds, the cut off for angle and distance was set to 120^0 and 3.5 Å, respectively. Figure 5A shows the total number of hydrogen bonds between the two monomers of Aβ$_{1-42}$ dimer. The total numbers of intermolecular hydrogen bonds were found to be 3. A large number of hydrophobic contacts ~ 350 were found to be involved in the stabilization of the dimer structure (Figure 5B).

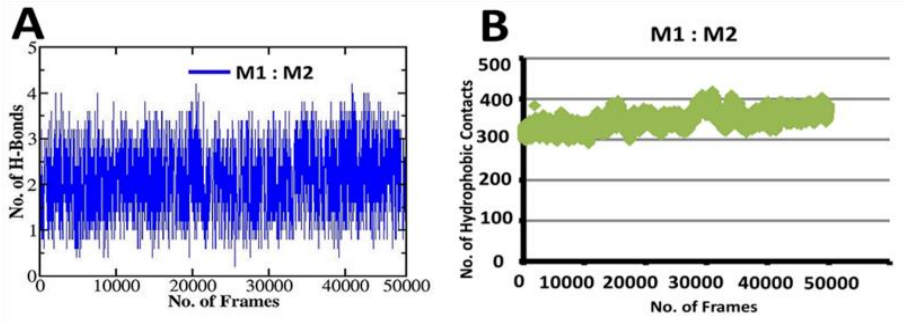

Figure 5. A) The total number of inter-molecular Hydrogen bonds; B) Total number of hydrophobic contacts vs total no. of frames for the Aβ_{1-42} dimer during the time course of simulation at 300K.

Similarly, the inter-molecular hydrogen bonds between the monomeric units of trimer and tetramer were calculated. Figure 6 shows the total number of intermolecular hydrogen bonds between the monomers of Aβ_{1-42} trimer. From Figure 6, we notice ~5 inter-molecular hydrogen bonds to stabilize the interaction between monomer 1 and 2 and ~2 inter-molecular hydrogen bonds to stabilize the interaction of monomer 3 with monomer 1 and 2.

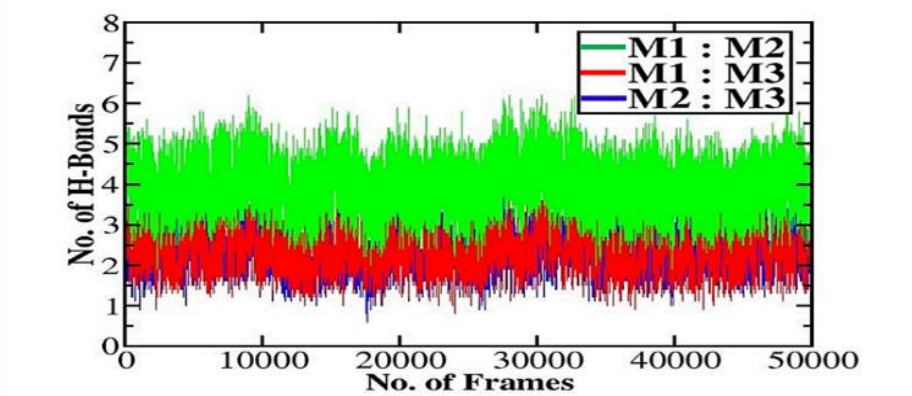

Figure 6. The total number of inter-molecular Hydrogen bonds vs. total no. of frames for the Aβ_{1-42} trimer during the time course of simulation at 300 K.

Likewise, the total numbers of intermolecular hydrogen bonds between the monomers of Aβ_{1-42} tetramer are illustrated in Figure 7. From Figure 7A, we observed monomer 1 to form ~6 and 3 inter-molecular hydrogen bonds with monomer 2 and monomer 4, respectively. Monomer 3 was found to form 3 inter-molecular hydrogen bonds with monomer 2 and 4 (Figure 7B).

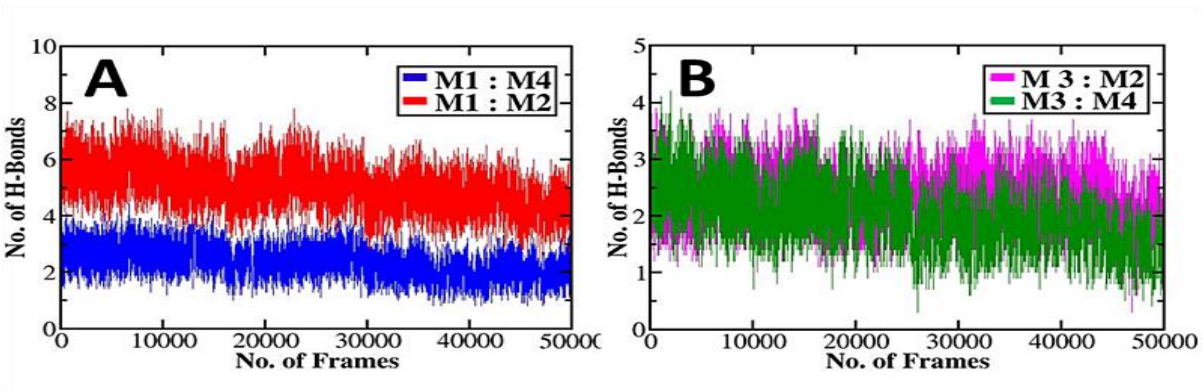

Figure 7. The total number of inter-molecular Hydrogen bonds vs. total no. of frames for the Aβ_{1-42} tetramer during the time course of simulation at 300 K.

We have further shown the acceptor and donor residues that were involved in the formation of the respective hydrogen-bonds in $A\beta_{1-42}$ dimer (Table 2), trimer (Table 3), and tetramer (Table 4).

Table 2. Inter-Molecular hydrogen bonding analysis of $A\beta_{1-42}$ dimer Aβ Monomer 1 (Acceptor): Aβ Monomer 2 (Donor)

Acceptor	Donor	Fraction
ASP_7	GLY_35	0.2448
SER_10	LYS_38	0.2217
GLY_13	ILE_42	0.084
ILE_15	ALA_40	0.0812
VAL_24	ALA_31	0.0716

Table 3. Inter-Molecular hydrogen bonding analysis of $A\beta_{1-42}$ trimer

A. Aβ Monomer 1 (Acceptor): Aβ Monomer 2 (Donor)

Acceptor	Donor	Fraction
ARG_5	GLU_64	0.2210
HIE_13	LEU_59	0.0986
ARG_5	GLU_64	0.0784
HIE_6	VAL_60	0.0775
HIE_6	GLU_64	0.697

B. Aβ Monomer 1 (Acceptor): Aβ Monomer 3 (Donor)

Acceptor	Donor	Fraction
VAL_36	GLU_99	0.3758
GLY_37	GLU_99	0.3600
LYS_28	ASP_91	0.0500
ALA21_6	GLY93_60	0.0441
MET_35	GLU_99	0.0429

C. Aβ Monomer 2 (Acceptor): Aβ Monomer 3 (Donor)

Acceptor	Donor	Fraction
GLU_64	ARG_89	0.3210
PHE_63	LYS_101	0.2986
PHE_62	ARG_89	0.1784
ILE_74	LEU_100	0.0775
GLY_76	GLY_136	0.0697

Table 4. Intermolecular hydrogen bonding analysis of $A\beta_{1-42}$ tetramer

A. Aβ Monomer 1 (Acceptor): Aβ Monomer 2 (Donor)

Acceptor	Donor	Fraction
ARG_5	ASP_49	0.3991
SER_8	SER_50	0.1677
HIE_13	GLU_64	0.1425
ARG_5	GLU_53	0.0954
LYS_16	ASP_65	0.0864

B. Aβ Monomer 1 (Acceptor): Aβ Monomer 3 (Donor)

Acceptor	Donor	Fraction
SER_8	VAL_96	0.0029
SER_8	HIE_97	0.0020
GLY_9	HIE_97	0.0005
LEU_34	ASN_111	0.0003
VAL_12	HIE_97	0.0003

C. Aβ Monomer 1 (Acceptor): Aβ Monomer 4 (Donor)

Acceptor	Donor	Fraction
LYS_16	ASP_149	0.0514
ILE_41	LYS_154	0.0500
HIE_14	ARG_131	0.0157
HIE_13	ARG_149	0.0032
HIE_13	ASP_127	0.0032

D. Aβ Monomer 2 (Acceptor): Aβ Monomer 3 (Donor)

Acceptor	Donor	Fraction
ARG_47	ASP_91	0.5271
HIE_48	GLU_95	0.4387
TYR_52	GLU_106	0.2635
HIE_55	ASP_107	0.1126
LYS_58	HIE_97	0.1101

E. Aβ Monomer 2 (Acceptor): Aβ Monomer 4 (Donor)

Acceptor	Donor	Fraction
ASP_49	ASP_133	0.1054
SER_50	SER_134	0.0910
HIE_48	GLU_129	0.0900
GLU_53	SER_134	0.0874
ASP_65	GLU_137	0.0638

F. Aβ Monomer 3 (Acceptor): Aβ Monomer 4 (Donor)

Acceptor	Donor	Fraction
MET_77	MET_152	0.1130
MET_77	GLY_157	0.1021
LEU_76	GLU_129	0.0865
VAL_78	SER_134	0.0844
LEU_76	GLU_137	0.0638

The hydrophobic contacts between different monomeric units in trimer and tetramer are shown in Figures 8 & 9, respectively. Thus it can be inferred that hydrogen bonding and hydrophobic are important in stabilizing the oligomers.

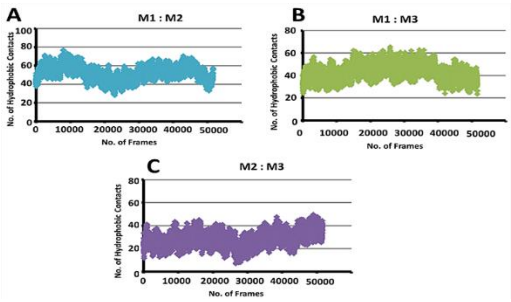

Figure 8. Total number of hydrophobic contacts vs. total no. of frames for the $A\beta_{1-42}$ trimer during the time course of simulation at 300 K.

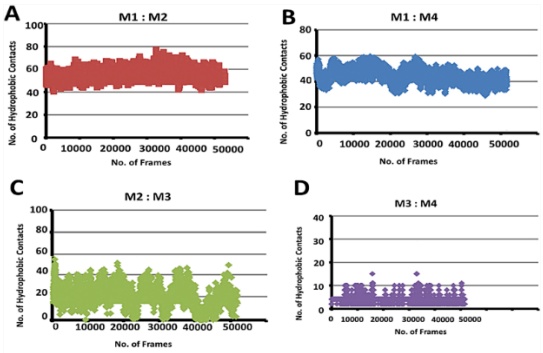

Figure 9. Total number hydrophobic contacts vs. total no. of frames for the $A\beta_{1-42}$ tetramer during the time course of simulation at 300 K

3.3. Interface statistics and residue-residue interaction study of $A\beta_{1-42}$ oligomers using the PDBSum server.

Additionally, using the PDBSum server, we have investigated the interface statistics and the residues involved in the formation of the $A\beta_{1-42}$ dimer. The interface statistics of $A\beta_{1-42}$ are provided in Table 5. The interface area of each of the monomers in the dimer was found to be in the range ~1000 $Å^2$. In the same manner, the total numbers of interface residues

involved in the interaction in both the chains were found to be twenty-one. The dimer was found to be stabilized by intermolecular hydrogen bonds (3) and non-bonded contacts (369), as shown in Table 5.

Table 5. The interface plot statistics of the Aβ_{1-42} dimer as predicted by the PDBSum server. A high number of non-bonded contacts indicate the existence of hydrophobic interaction in the dimer.

Chain	No. of Interface Residues	Interface Area (Å^2)	No. of Salt Bridges	No. of Hydrogen Bonds	No. of Non-bonded Contacts
A : B	21 : 21	998 : 1011	0	3	369

In Figure 10, we have summarized the residues involved in the intermolecular interaction in the Aβ_{1-42} dimer.

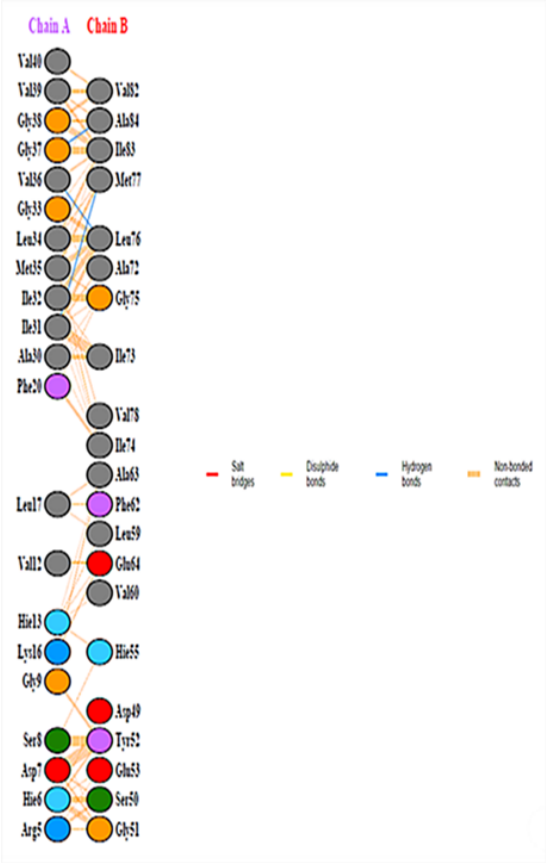

Figure 10. The interface residues of the Aβ_{1-42} dimer as summarized by the PDBSum server.

We noticed most of the Central hydrophobic core and C-terminal region residues to be involved in the interactions. A few N-terminal residues were also noticed to form hydrogen bonds and non-bonded contacts. The interface statistics of the Aβ_{1-42} trimer is provided in Table 6. As shown in Table 6, a large number of non-bonded contacts, seven hydrogen bonds, and three salt bridges were found to aid in the association of monomeric units to form a stabilized trimer structure.

Table 6. The interface plot statistics of the Aβ_{1-42} trimer as predicted by the PDBSum server.

Chain	No. of Interface Residues	Interface Area (Å^2)	No. of Salt Bridges	No. of Hydrogen Bonds	No. of Non-bonded Contacts
A : B	12 : 12	733 : 668	2	4	63
A : C	9 : 9	609 : 590	0	3	40
B : C	8 : 8	418 : 411	1	2	35

The interface area was found to be highest between chains A and chain B, which is ~700 Å^2. Furthermore, we have highlighted the residues involved in the formation of the inter-peptide salt bridges of the monomeric units of Aβ_{1-42} trimer in Table 7.

Table 7. The inter-peptide Salt bridge analysis of the Aβ_{1-42} trimer as predicted by the PDBSum server.

Chain	Atom No.	Residue name	Atom name	Residue No.		Atom No.	Residue name	Atom name	Residue No.
A : B	79	ARG	NH2	5	⟷	981	GLU	OE2	64
A : B	163	GLU	OE1	11	⟷	1060	LYS	NZ	70
B : C	640	ASP	OD2	43	⟷	1688	LYS	NZ	112

Likewise, we carried out the protein-protein interaction studies in the PDBSum server for the full-length Aβ_{1-42} tetramer structure. Different interactions that play a crucial role in the tetramer formation are shown in Table 8.

Table 8. The interface plot statistics of the Aβ_{1-42} tetramer as predicted by the PDBSum server.

Chain	No. of Interface Residues	Interface Area (Å^2)	No. of Salt Bridges	No. of Hydrogen Bonds	No. of Non-bonded Contacts
A : B	7 : 11	533 : 496	3	6	65
A : D	8 : 8	442 : 447	1	3	50
B : C	5 : 6	345 : 347	1	4	33
B : D	1 : 1	73 : 74	0	0	4
C : D	5 : 5	319 : 356	1	3	8

Six inter-peptide salt bridges were found to stabilize the tetramer structure. A total of sixteen inter-molecular hydrogen bonds and a large number of non-bonded contacts were found to stabilize the tetramer structure. Furthermore, we have highlighted the residues involved in the formation of the inter-peptide salt bridges of the monomeric units of Aβ_{1-42} tetramer, as shown in Table 9.

Table 9. The inter-peptide salt bridge analysis of the Aβ_{1-42} tetramer as predicted by the PDBSum server.

Chain	Atom No.	Residue name	Atom name	Residue No.		Atom No.	Residue name	Atom name	Residue No.
A : B	73	ARG	NE	5	⟷	980	GLU	OE1	64
A : B	79	ARG	NH2	5	⟷	981	GLU	OE2	64
A : B	163	GLU	NZ	11	⟷	1060	LYS	NZ	70
A : B	627	ALA	OXT	42	⟷	707	ARG	NH2	47
A : C	536	VAL	N	36	⟷	1484	GLN	OE1	99
A : C	552	GLY	N	37	⟷	1484	GLN	OE1	99
B : C	723	HIE	NE2	48	⟷	1609	GLU	OE2	106

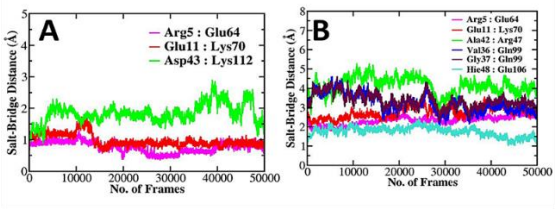

Figure 11. Inter-peptide salt-bridge vs. the total number of frames for A) Aβ_{1-42} trimer; B) Aβ_{1-42} tetramer during the time course of simulation at 300 K.

Additionally, we have carried out salt-bridge analysis from the MD trajectories to ensure the data obtained from the PDBSum by measuring the distance between the center of mass of the residues that formed the salt-bridges in trimer and tetramer. Salt bridge that normally exists in Aβ_{1-42} peptide has been reported to play an important role in stabilizing the peptide structure. From Figure 11, we can see that the distance between the center of mass of the residues to be less than 5 Å at a certain time period of simulation, which validated the salt bridge [49].

Thus the salt-bridges that were reported to be formed between the monomeric units in the trimer and tetramer complexes by PDBSum server were found to be valid, and thus they might play an important role in stabilizing the oligomers.

4. Conclusions

Due to flexibility and high susceptibility to aggregation, the low molecular weight, toxic $A\beta_{1-42}$ oligomers are not easy to study. In this work, we have carried out all-atom MD simulations on full-length $A\beta_{1-42}$ dimer, trimer, and tetramer and further studied the interactions that hold together the individual monomeric units. Our results suggest that the formation of a stable $A\beta_{1-42}$ oligomer occurs through secondary structural transitions from α-helix to random coils. In the intermediate stages, Aβ dimer, trimer, and tetramer have already acquired random coil structures. The oligomers formed are thus random coil rich, which may further form β-strands. The conformations observed in our study may represent transient structures that may result during the course of oligomerization of $A\beta_{1-42}$ peptide. From the interaction study, we found an inter-peptide salt bridge, hydrogen bonds, and non-bonded contacts to play a crucial role in stabilizing the oligomers. Additionally, the CHC region and C-terminal region were found to be involved in the intermolecular interactions in the oligomers.

Funding

This research received no external funding.

Acknowledgments

We would like to thank the Tezpur University for the start-up grant and DBT funded Bioinformatics Infrastructure facility in the Department of Molecular Biology and Biotechnology at Tezpur University for providing us computational facility to carry out this research work.

Conflicts of Interest

The authors declare no conflict of interest.

References

1. Ambrose, C.T. A therapeutic approach for senile dementias: neuroangiogenesis. *J Alzheimers Dis* **2015,** *43*, 1-17, https://doi.org/10.3233/jad-140498.
2. Satizabal, C.L.; Beiser, A.S.; Chouraki, V.; Chêne, G.; Dufouil, C.; Seshadri, S. Incidence of dementia over three decades in the Framingham Heart Study. *N Engl J Med* **2016,** *374*, 523-532, https://doi.org/10.1056/nejmc1604823
3. Selkoe, D.J.; Hardy, J. The amyloid hypothesis of Alzheimer's disease at 25 years. *EMBO mol Med* **2016,** *8*, 595-608. https://doi.org/10.1111/j.1471-4159.2009.06181.x.
4. Kuruva, C.S.; Reddy, P.H. Amyloid beta modulators and neuroprotection in Alzheimer's disease: a critical appraisal. *Drug Discov. Today* **2017,** *22*, 223-233, https://doi.org/10.1016/j.drudis.2016.10.010.
5. Wilson, E.N.; Abela, A.R.; Do Carmo, S.; Allard, S.; Marks, A.R.; Welikovitch, L.A.; Ducatenzeiler, A.; Chudasama, Y.; Cuello, A.C. Intraneuronal amyloid beta accumulation disrupts hippocampal CRTC1-dependent gene expression and cognitive function in a rat model of Alzheimer disease. *Cereb Cortex* **2017,** *27*, 1501-1511, https://doi.org/10.1093/cercor/bhv332.
6. Liu, L.; Niu, L.; Xu, M.; Han, Q.; Duan, H.; Dong, M.; Besenbacher, F.; Wang, C.; Yang, Y. Molecular tethering effect of C-terminus of amyloid peptide Aβ42. *ACS nano* **2014,** *8*, 9503-9510, https://doi.org/10.1021/nn503737r.
7. Lednev, I.K.; Kurouski, D. Amyloid fibril polymorphism probed by advanced vibrational spectroscopy. *J Biomol Struct Dyn* **2013,** *31*, 94-95, https://doi.org/10.1080/07391102.2013.786388.

8. Pham, J.D.; Chim, N.; Goulding, C.W.; Nowick, J.S. Structures of Oligomers of a Peptide from β-Amyloid. *J. Am. Chem. Soc* **2013**, *135*, 12460-12467, https://doi.org/10.1021/ja4068854.
9. Zhao, L.N.; Long, H.; Mu, Y.; Chew, L.Y. The Toxicity of Amyloid β Oligomers. *Int J Mol Sci* **2012,** *13*, 7303-7327, https://doi.org/10.3390/ijms13067303.
10. Ferreira, S.T.; Lourenco, M.V.; Oliveira, M.M.; De Felice, F.G. Soluble amyloid-β oligomers as synaptotoxins leading to cognitive impairment in Alzheimer's disease. *Front Cell Neurosci* **2015,** *9*, https://doi.org/10.3389/fncel.2015.00191.
11. Hefti, F.; Goure, W.F.; Jerecic, J.; Iverson, K.S.; Walicke, P.A.; Krafft, G.A. The case for soluble Aβ oligomers as a drug target in Alzheimer's disease. *Trends Pharmacol Sci* **2013,** *34*, 261-266, https://doi.org/10.1016/j.tips.2013.03.002.
12. Leahy, C.T.; Murphy, R.D.; Hummer, G.; Rosta, E.; Buchete, N.V. Coarse master equations for binding kinetics of amyloid peptide dimers. *J Phys Chem Lett* **2016,** *7*, 2676-2682, https://doi.org/10.1021/acs.jpclett.6b00518.
13. Chang, L.K.; Zhao, J.H.; Liu, H.L.; Wu, J.W.; Chuang, C.K.; Liu, K.T.; Chen, J.T.; Tsai, W.B.; Ho, Y. The importance of steric zipper on the aggregation of the MVGGVV peptide derived from the amyloid β peptide. *J Biomol Struct Dyn* **2010,** *28*, 39-50, https://doi.org/10.1080/07391102.2010.10507342.
14. Lührs, T.; Ritter, C.; Adrian, M.; Riek-Loher, D.; Bohrmann, B.; Döbeli, H.; Schubert, D.; Riek, R. 3D structure of Alzheimer's amyloid-β (1–42) fibrils. *Proc Natl Acad Sci USA* **2005,** *102*, 17342-17347, https://doi.org/10.1073/pnas.0506723102.
15. Makin, O.S.; Atkins, E.; Sikorski, P.; Johansson, J.; Serpell, L.C. Molecular basis for amyloid fibril formation and stability. *Proc Natl Acad Sci USA* **2005,** *102*, 315-320, https://doi.org/10.1073/pnas.0406847102.
16. Xu, W.; Zhang, C.; Derreumaux, P.; Gräslund, A.; Morozova-Roche, L.; Mu, Y. Intrinsic Determinants of Aβ12–24 pH-dependent self-assembly revealed by combined computational and experimental studies. *PLoS One* **2011,** *6*, https://doi.org/10.1371/journal.pone.0024329.
17. Salahuddin, P.; Fatima, M.T.; Abdelhameed, A.S.; Nusrat, S.; Khan, R.H. Structure of amyloid oligomers and their mechanisms of toxicities: targeting amyloid oligomers using novel therapeutic approaches. *Eur J Med Chem* **2016,** *114*, 41-58, https://doi.org/10.1016/j.ejmech.2016.02.065.
18. Tarczyluk, M.A.; Nagel, D.A.; Parri, H.R.; Tse, E.H.; Brown, J.E.; Coleman, M.D.; Hill, E.J. Amyloid β 1-42 induces hypometabolism in human stem cell-derived neuron and astrocyte networks. *Cereb Blood Flow Metab* **2015,** *35*, 1348-1357, https://doi.org/10.1038/jcbfm.2015.58.
19. Breydo, L.; Kurouski, D.; Rasool, S.; Milton, S.; Wu, J.W.; Uversky, V.N.; Lednev, I.K.; Glabe, C.G. Structural differences between amyloid beta oligomers. *Biochem Biophys Res Commun* **2016,** *477*, 700-705, https://doi.org/10.1016/j.bbrc.2016.06.122.
20. Kakio, A.; Nishimoto, S.I.; Yanagisawa, K.; Kozutsumi, Y.; Matsuzaki, K. Interactions of amyloid β-protein with various ganglioside-bound form as an endogenous seed for Alzheimer amyloid. *Biochemistry* **2002,** *41*, 7385-7390, https://doi.org/10.1021/bi0255874.
21. Huang, D.; Zimmerman, M.I.; Martin, P.K.; Nix, A.J.; Rosenberry, T.L.; Paravastu, A.K. Antiparallel β-sheet structure within the C-terminal region of 42-residue Alzheimer's amyloid-β peptides when they form 150-kDa oligomers. *J Mol Biol* **2015,** *427*, 2319-2328, https://doi.org/10.1016/j.jmb.2015.04.004.
22. Barz B.; Urbanc, B. Dimer formation enhances structural differences between amyloid β-protein (1–40) and (1–42): an explicit-solvent molecular dynamics study. *PloS one* **2012,** *7*, https://doi.org/10.1371/journal.pone.0034345.
23. Shea, D.; Hsu, C.C.; Bi, T.M.; Paranjapye, N.; Childers, M.C.; Cochran, J.; Tomberlin, C.P.; Wang, L.; Paris, D.; Zonderman, J.; Varani, G.; Link, C.D.; Mullan, M.; Daggett, V. α-sheet secondary structure in amyloid β-peptide drives aggregation and toxicity in Alzheimer's disease. *Proc Natl Acad Sci USA* **2019,** *116*, 8895-8900, https://doi.org/10.1073/pnas.1820585116.
24. Yu, X.; Zheng, J. Polymorphic structures of Alzheimer's β-amyloid globulomers. *PloS one* **2011,** *6*, https://doi.org/10.1371/journal.pone.0020575.
25. Kuperstein, I.; Broersen, K.; Benilova, I.; Rozenski, J.; Jonckheere, W.; Debulpaep, M.; Vandersteen, A.; Segers-Nolten, I.; Van Der Werf, K.; Subramaniam, V.; Braeken, D. Neurotoxicity of Alzheimer's disease Aβ peptides is induced by small changes in the Aβ 42 to Aβ 40 ratio. *EMBO J* **2010,** *9*, 3408-3420, https://doi.org/10.1038/emboj.2010.211.
26. Stroud, J.C.; Liu, C.; Teng, P.K.; Eisenberg, D. Toxic fibrillar oligomers of amyloid-β have cross-β structure. *Proc Natl Acad Sci USA* **2012,** *109*, 7717-7722, https://doi.org/10.1073/pnas.1203193109.
27. Festa, G.; Mallamace, F.; Sancesario, G. M.; Corsaro, C.; Mallamace, D.; Fazio, E.; Arcidiacono, L.; Garcia Sakai, V.; Senesi, R.; Preziosi, E.; Sancesario, G.; Andreani, C. Aggregation States of A$\beta_{1\text{-}40}$, A$\beta_{1\text{-}42}$ and Aβp$_{3\text{-}42}$ Amyloid Beta Peptides: A SANS Study. *Int J Mol Sci* **2019**, *20*, https://doi.org/10.3390/ijms20174126.
28. Ciccone, L.; Shi, C.; di Lorenzo, D.; Van Baelen, A.C.; Tonali, N. The Positive Side of the Alzheimer's Disease Amyloid Cross-Interactions: The Case of the Aβ 1-42 Peptide with Tau, TTR, CysC, and ApoA1. *Molecules (Basel, Switzerland)* **2020**, *25*, https://doi.org/10.3390/molecules25102439.

29. Fabiani, C.; Antollini, S.S. Alzheimer's Disease as a Membrane Disorder: Spatial Cross-Talk Among Beta-Amyloid Peptides, Nicotinic Acetylcholine Receptors and Lipid Rafts. *Front Cell Neurosci*. **2019**, *13*, https://doi.org/10.3389/fncel.2019.00309.
30. Ezpeleta, J.; Baudouin, V.; Arellano-Anaya, Z.E.; Boudet-Devaud, F.; Pietri, M.; Baudry, A.; Haeberlé, A.M.; Bailly, Y.; Kellermann, O.; Launay, J.M.; Schneider, B. Production of seedable Amyloid-β peptides in model of prion diseases upon PrP^{Sc}-induced PDK1 overactivation. *Nat. Commun.* **2019**, *10*, https://doi.org/10.1038/s41467-019-11333-3.
31. Man, V. H.; He, X.; Ji, B.; Liu, S.; Xie, X.Q.; Wang, J. Molecular Mechanism and Kinetics of Amyloid-β_{42} Aggregate Formation: A Simulation Study. *ACS Chem Neurosci* **2019**, *10*, 4643–4658, https://doi.org/10.1021/acschemneuro.9b00473.
32. Lazzaro, S.; Ogrinc, N.; Lamont, L.; Vecchio, G.; Pappalardo, G.; Heeren, R. Ion mobility spectrometry combined with multivariate statistical analysis: revealing the effects of a drug candidate for Alzheimer's disease on Aβ1-40 peptide early assembly. *Anal Bioanal Chem* **2019,** *411*, 6353–6363, https://doi.org/10.1007/s00216-019-02030-7.
33. Han, K.; Kim, S. H.; Choi, M. Computational modeling of the effects of autophagy on amyloid-β peptide levels. *Theor Biol Med Model.* **2020,** *17*, https://doi.org/10.1186/s12976-020-00119-6.
34. Ahmad, S.S.; Khan, H.; Danish Rizvi, S.M.; Ansari, S.A.; Ullah, R.; Rastrelli, L.; Mahmood, H.M.; Siddiqui, M.H. Computational Study of Natural Compounds for the Clearance of Amyloid-Beta: A Potential Therapeutic Management Strategy for Alzheimer's Disease. *Molecules (Basel, Switzerland*) **2019**, *24*, https://doi.org/10.3390/molecules24183233.
35. Köppen, J.; Schulze, A.; Machner, L.; Wermann, M.; Eichentopf, R.; Guthardt, M.; Hähnel, A.; Klehm, J.; Kriegeskorte, M.C.; Hartlage-Rübsamen, M.; Morawski, M.; von Hörsten, S.; Demuth, H.U.; Roßner, S.; Schilling, S. Amyloid-Beta Peptides Trigger Aggregation of Alpha-Synuclein In Vitro. *Molecules (Basel, Switzerland)* **2020**, *25*, https://doi.org/10.3390/molecules25030580.
36. Raimundo, A.F.; Ferreira, S.; Martins, I. C.; Menezes, R. Islet Amyloid Polypeptide: A Partner in Crime With Aβ in the Pathology of Alzheimer's Disease. *Front Mol Neurosci* **2020,** *13*, https://doi.org/10.3389/fnmol.2020.00035.
37. Pierce, B.; Tong, W.; Weng, Z. M-ZDOCK: A Grid-based Approach for Cn Symmetric Multimer Docking. *Bioinformatics* **2005,** *21*, 1472-1476, https://doi.org/10.1093/bioinformatics/bti229.
38. Laskowski, R.A.; Hutchinson, E.G.; Michie, A.D.; Wallace, A.C.; Jones, M.L.; Thornton, J.M. PDBsum: a Web-based database of summaries and analyses of all PDB structures. *Trends Biochem Sci* **1997,** *22*, 488-490, https://doi.org/10.1016/s0968-0004(97)01140-7.
39. Crescenzi, O.; Tomaselli, S.; Guerrini, R.; Salvadori, S.; D'Ursi, A.M.; Temussi, P.A.; Picone, D. Solution structure of the Alzheimer amyloid β-peptide (1–42) in an apolar microenvironment. *Eur J Biochem* **2002,** *269*, 5642-5648, https://doi.org/10.1046/j.1432-1033.2002.03271.x.
40. Jorgensen, W. L.; Jenson, C. Temperature dependence of TIP3P, SPC, and TIP4P water from NPT Monte Carlo simulations: Seeking temperatures of maximum density. *J Comput Chem* **1998,** *19*, 1179-1186, https://doi.org/10.1002/(sici)1096-987x(19980730)19:10%3C1179::aid-jcc6%3E3.0.co;2-j.
41. Ryckaert. J.P.; Ciccotti, G.; Berendsen, H.J. Numerical integration of the cartesian equations of motion of a system with constraints: molecular dynamics of n-alkanes. *J Comput Phys* **1977,** *23*, 327-341, https://doi.org/10.1016/0021-9991(77)90098-5.
42. Berendsen, H.J.; Postma, J.V.; van Gunsteren, WF.; DiNola, A.R.; Haak, J.R. Molecular dynamics with coupling to an external bath. *J Chem Phys* **1984,** *81*, 3684-3690, https://doi.org/10.1063/1.448118.
43. Darden, T.; York, D.; Pedersen, L. Particle mesh Ewald: An N· log (N) method for Ewald sums in large systems. *J Chem Phys* **1993,** *98,* 10089-10092, https://doi.org/10.1063/1.464397.
44. Kakati, M.; Das, D.; Das, P.; Sanjeev, A.; Mattaparthi, V.S.K. Effect of ethanol as molecular crowding agent on the conformational dynamics of α-synuclein. *Lett. Appl. NanoBioscience* **2020**, *9*, 779-783, https://doi.org/10.33263/LIANBS91.779783.
45. Feig, M.; Karanicolas, J.; Brooks, C.L. MMTSB Tool Set: enhanced sampling and multiscale modeling methods for applications in structural biology. *J Mol Graph Model* **2004,** *22*, 377-395, https://doi.org/10.1016/j.jmgm.2003.12.005.
46. Humphrey, W.; Dalke, A.; Schulten, K. VMD: visual molecular dynamics. *J mol graphics* **1996,** *14*, 33-38, https://doi.org/10.1016/0263-7855(96)00018-5.
47. Kabsch, W.; Sander, C. Dictionary of protein secondary structure: pattern recognition of hydrogen-bonded and geometrical features. *Biopolymers* **1983**, *22*, 2577-2637, https://doi.org/10.1002/bip.360221211.
48. Krieger, E.; Vriend, G. New ways to boost molecular dynamics simulations. *J Comput Chem* **2015,** *36,* 996-1007, https://doi.org/10.1002/jcc.23899.
49. Marqusee, S.; Baldwin, R.L. (1987) Helix stabilization by Glu-... Lys+ salt bridges in short peptides of de novo design. *Proc Natl Acad Sci USA* **1987,** *84*, 8898-8902, https://doi.org/10.1073/pnas.84.24.8898.

Supplementary files

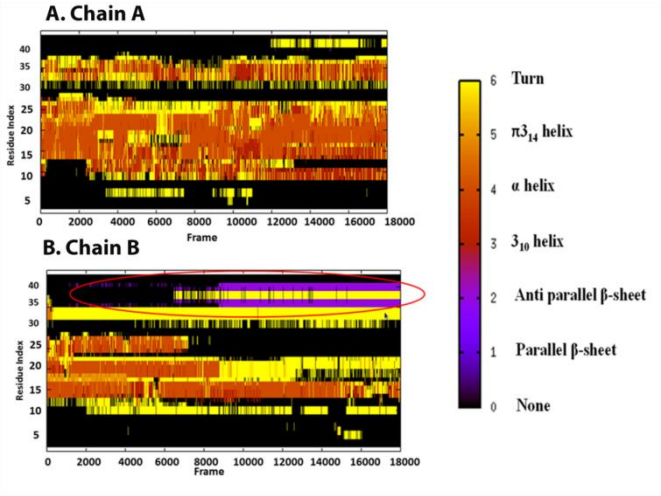

Figure S1. Time evolution of Secondary structure of Amyloid $\beta_{1\text{-}42}$ dimer at 300 K. The encircled area in red shows the appearance of β-strands.

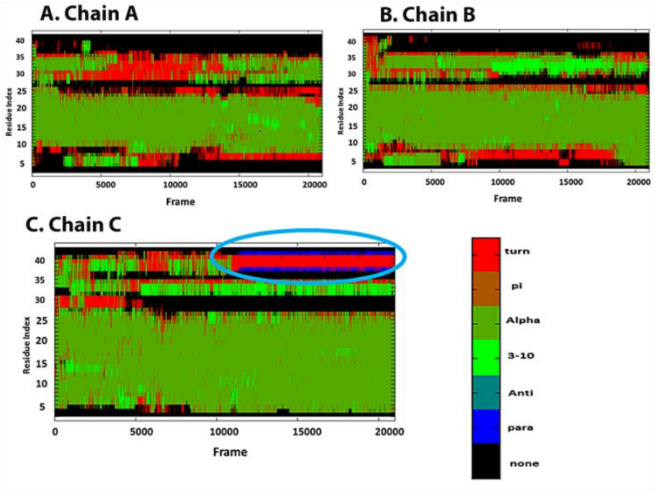

Figure S2. Time evolution of Secondary structure of Amyloid $\beta_{1\text{-}42}$ trimer at 300 K. The encircled area in blue shows the appearance of β-strands.

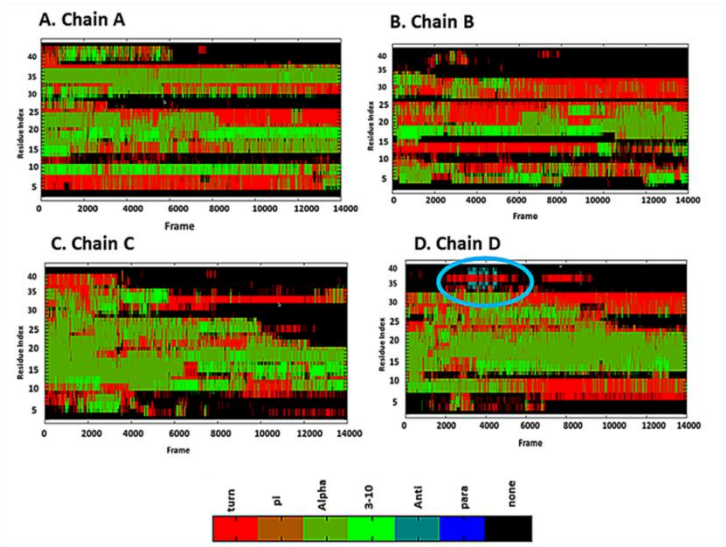

Figure S3. Time evolution of Secondary structure of Amyloid $\beta_{1\text{-}42}$ tetramer at 300 K. The encircled area in blue shows the appearance of β-strands.